ACS OMEGA

http://pubs.acs.org/journal/acsodf

Article

Heme-Thiolate Perturbation in Cystathionine β-Synthase by Mercury Compounds

Dayana Benchoam, Ernesto Cuevasanta, Laia Julió Plana, Luciana Capece, Ruma Banerjee, and Beatriz Alvarez*

Cite This: *ACS Omega* 2021, 6, 2192−2205

Read Online

ACCESS | Metrics & More | Article Recommendations

ABSTRACT: Cystathionine β-synthase (CBS) is an enzyme involved in sulfur metabolism that catalyzes the pyridoxal phosphate-dependent condensation of homocysteine with serine or cysteine to form cystathionine and water or hydrogen sulfide (H_2S), respectively. CBS possesses a *b*-type heme coordinated by histidine and cysteine. Fe(III)-CBS is inert toward exogenous ligands, while Fe(II)-CBS is reactive. Both Fe(III)- and Fe(II)-CBS are sensitive to mercury compounds. In this study, we describe the kinetics of the reactions with mercuric chloride ($HgCl_2$) and *p*-chloromercuribenzoic acid. These reactions were multiphasic and resulted in five-coordinate CBS lacking thiolate ligation, with six-coordinate species as intermediates. Computational QM/MM studies supported the feasibility of formation of species in which the thiolate is proximal to both the iron ion and the mercury compound. The reactions of Fe(II)-CBS were faster than those of Fe(III)-CBS. The observed rate constants of the first phase increased hyperbolically with concentration of the mercury compounds, with limiting values of 0.3−0.4 s^{-1} for Fe(III)-CBS and 40 ± 4 s^{-1} for Fe(II)-CBS. The data were interpreted in terms of alternative models of conformational selection or induced fit. Exposure of Fe(III)-CBS to $HgCl_2$ led to heme release and activity loss. Our study reveals the complexity of the interactions between mercury compounds and CBS.

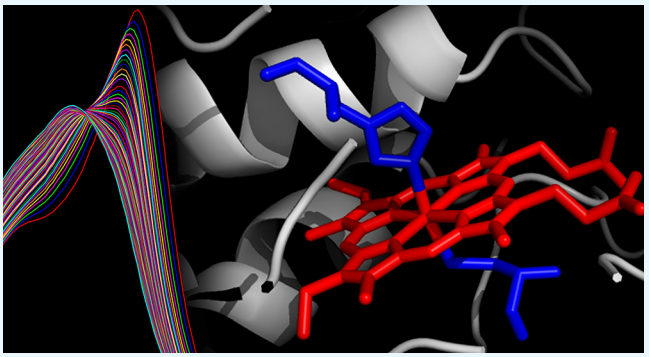

INTRODUCTION

Cystathionine β-synthase (CBS, UniProtKB P35520) is a key enzyme in the metabolism of sulfur amino acids in mammals. It catalyzes the first step of the transsulfuration pathway, the condensation of serine with homocysteine to form cystathionine and water. Alternatively, CBS condenses cysteine with homocysteine resulting in cystathionine and hydrogen sulfide (H_2S), a signaling molecule that modulates diverse cellular processes involving the nervous, cardiovascular, and gastrointestinal systems.[1,2] CBS also catalyzes the β-substitution of cysteine with water or a second molecule of cysteine to produce H_2S and serine or lanthionine, respectively. However, the physiological contribution of these reactions is minimal.[3] In addition, CBS catalyzes the formation of cysteine persulfide, pyruvate, and ammonium from cystine.[4,5] An elevated level of homocysteine in plasma is considered a risk factor for cardiovascular diseases, neural tube defects, and neurodegenerative diseases (*i.e.*, Alzheimer's disease).[6−9] Mutations in CBS are the most common cause of hereditary homocystinuria.[10]

Human CBS exists as a homodimer or as higher order oligomers.[11−14] Each subunit is formed by 551 amino acids and has a molecular weight of ∼63 kDa.[15] It presents a modular organization that consists of an N-terminal domain that binds heme (residues 1−70), a catalytic domain that binds pyridoxal 5′-phosphate (PLP) (residues 71−413), and a C-terminal regulatory domain (residues 414−551).[16−18] The first 40 residues constitute an intrinsically disordered region, which might be important for heme binding.[19] The allosteric activator *S*-adenosyl-L-methionine binds to the regulatory domain, increasing the enzymatic activity.[20]

CBS is the only known PLP-dependent enzyme that possesses a heme cofactor. In human CBS, heme is *b*-type and iron is low-spin and six-coordinate in both ferric (Fe(III)-CBS) and ferrous (Fe(II)-CBS) states.[17,21] The axial ligands are the thiolate of Cys52 and the $N_{\varepsilon 2}$ atom of His65.[22−24] The thiolate is within hydrogen-bonding distance of the guanidinium group of Arg266 and the amide backbone of Trp54.[23] The heme environment is conserved in eukaryotic species, but

Received: November 9, 2020
Accepted: December 22, 2020
Published: January 14, 2021

it does not resemble other heme proteins.[25] The catalytic role of heme has been excluded since it is located ∼20 Å from the PLP.[24,26] Furthermore, the CBS of *Trypanosoma cruzi* and yeast catalyze the same reaction as those of vertebrates and do not have heme.[27,28] A structural role has been assigned to this heme.[29] In addition, a regulatory role has been proposed since perturbations in the heme coordination decrease the enzymatic activity. Heme and PLP are connected via an α-helix that interacts with the heme ligand Cys52 through Arg266 and with the phosphate of PLP through two conserved threonine residues (Thr257 and Thr260). It has been proposed that alterations in the heme environment affect the PLP tautomeric equilibrium that modulates the activity.[30−33] The function of heme remains an intriguing issue.

The C-terminal regulatory domain of CBS can be removed by treatment with trypsin or by protein engineering. The truncated enzyme is not activated by *S*-adenosyl-L-methionine but is more active than full-length CBS and forms homodimers with 45 kDa subunits.[34,35] The UV−visible absorption spectra of the truncated and full-length CBS are identical and are dominated by heme.[21] The spectrum of Fe(III)-CBS exhibits a Soret peak at 428 nm and an α/β broad band centered at 550 nm. Upon reduction to Fe(II)-CBS, the Soret peak shifts to 449 nm and the broad band resolves into two peaks at 540 and 571 nm.[22,36,37]

Fe(III)-CBS is stable and inert toward typical ferric heme exogenous ligands. However, it is sensitive to the mercuric ion (Hg^{2+}) and high concentrations of peroxynitrite ($ONOO^-$, ∼150 μM).[21,22,38−40] It is also sensitive to nitric oxide ($NO^{\cdot}$), although with very slow kinetics.[41] In the absence of oxygen, Fe(III)-CBS can be reduced to Fe(II)-CBS by strong reductants such as sodium dithionite. It can also be reduced by methionine synthase reductase (MSR) in the presence of carbon monoxide (CO) and NADPH as the electron donor.[42,43] The ferrous heme is unstable and labile and can react with multiple molecules such as O_2, CO, $NO^{\cdot}$, CN^-, nitrite (NO_2^-), and mercury compounds.[21,38,40−50] In addition, Fe(II)-CBS can slowly decay into an inactive six-coordinate species that absorbs at 424 nm, where the cysteine is replaced by an unidentified neutral ligand.[51,52] The binding of CO and $NO^{\cdot}$ can lead to activity inhibition,[41,46,47,49,53] and it has been suggested that this inhibition could play pathophysiological roles.[54−59] In the case of CO, dissociation of Cys52 appears to be a prerequisite for the binding. The Cys52 dissociation rate constant in Fe(II)-CBS was estimated from the limiting rate constant for CO binding to be 0.003−0.017 s^{-1} at 25 °C and pH 7.0−8.6.[41,42,45,53] For the Cys52 association rate constant, a value of $\sim 10^3$ s^{-1} was determined based on resonance Raman-flash photolysis experiments with CO-bound Fe(II)-CBS.[45] There are no reports about the dissociation or the association rate constants of Cys52 in Fe(III)-CBS. In addition to Cys52, which provides the heme ligand, truncated CBS has nine other cysteines, of which only one, Cys15, can be titrated with 5,5′-dithiobis-(2-nitrobenzoic acid). This residue is not critical for activity.[11,39] It has been suggested that the formation of a disulfide bond between Cys272 and Cys275 leads to decreased activity.[60]

The thiophilic compound mercuric chloride ($HgCl_2$) alters the UV−visible absorption spectrum of Fe(III)-CBS.[22] When $HgCl_2$ is mixed with truncated Fe(III)-CBS, the Soret peak at 428 nm shifts to a wide peak at ∼395 nm. This shift is accompanied by loss of enzyme activity and is consistent with the conversion of the six-coordinate low-spin ferric ion to a five-coordinate high-spin complex, suggesting the loss of the thiolate ligand. The subsequent addition of homocysteine and other thiols to $HgCl_2$-exposed Fe(III)-CBS results in the formation of a six-coordinate species with a Soret maximum at 424 nm.[21,38] The addition of *p*-chloromercuribenzoic acid (*p*-CMB) to Fe(III)-CBS also inhibits the enzyme activity, which is relieved by the addition of thiols.[61] In the case of Fe(II)-CBS, $HgCl_2$ induces the formation of a species with a maximum at 425 nm, consistent with the formation of a six-coordinate species lacking the thiolate ligand. Therefore, it is suggested that the cysteine is replaced by an unknown ligand. The species formed do not show enzyme activity.[21,38] Moreover, when *p*-CMB is added to Fe(II)-CBS, the maximum shifts from 449 to 428 nm with an isosbestic point at 438 nm.[50]

In this study, we characterized the kinetics of the reactions of Fe(III)-CBS and Fe(II)-CBS with mercury compounds with the aim of investigating the kinetics of the heme-thiolate interaction and determining the rate constant for thiolate dissociation from heme, which, in the case of Fe(II)-CBS, appears relevant for modulation by CO.

MATERIALS AND METHODS

Enzyme Purification. Truncated human CBS lacking 143 amino acids at the C-terminus was purified from an *Escherichia coli* expression system (pGEX4T1/hCBSΔC143) that produces a fusion protein with glutathione transferase. The protein was purified as described previously using affinity chromatography with glutathione sepharose,[33,37] and the glutathione transferase tag was removed using thrombin. The concentration of CBS in phosphate buffer (0.2 M, pH 7.4) was determined from the absorbance at 428 nm using the extinction coefficient based on heme (ε_{428} = 92,700 ± 4600 M^{-1} cm^{-1}).[44] The protein was stored in the mentioned buffer at −80 °C prior to use.

Mercury Compounds. $HgCl_2$, *p*-CMB, and *p*-hydroxymercuribenzoic acid (*p*-HMB) were purchased from Sigma-Aldrich. Stock solutions of $HgCl_2$ were prepared in distilled water, *p*-CMB, and *p*-HMB in 0.05−0.1 M NaOH followed by neutralization with HCl. Since the buffer used in the experiments was Tris−HCl (0.1 M, pH 7.4), the mercury compounds were coordinated with chlorides in the working solutions according to the equilibrium constants and concentrations,[62,63] and the use of *p*-HMB was equivalent to the use of *p*-CMB. Moreover, the chlorides are labile and exchange rapidly with other ligands such as thiolates.[63,64]

Kinetics of the Reaction of Fe(III)-CBS with Mercury Compounds. The kinetics of the reactions between Fe(III)-CBS and mercury compounds were followed in Tris−HCl buffer (0.1 M, pH 7.4) at 25 °C by UV−visible absorption spectroscopy (Varian Cary 50 spectrophotometer or Varioskan Flash plate reader). Rapid kinetics were studied using a stopped-flow accessory (Applied Photophysics RX2000) coupled to the spectrophotometer. Data were analyzed with the OriginPro 8 software.

Kinetics of the Reaction of Fe(II)-CBS with *p*-CMB. Fe(II)-CBS was generated by titration of Fe(III)-CBS in Tris−HCl buffer (0.1 M, pH 7.4) with sodium dithionite in a tonometer under a nitrogen atmosphere. To avoid an excess of dithionite, the minimum amount needed for reduction was used and monitored by the appearance of the characteristic Fe(II)-CBS peak at 449 nm. The sodium dithionite stock was diluted in oxygen-free 0.1 M NaOH and quantified by

https://dx.doi.org/10.1021/acsomega.0c05475
ACS Omega 2021, 6, 2192−2205

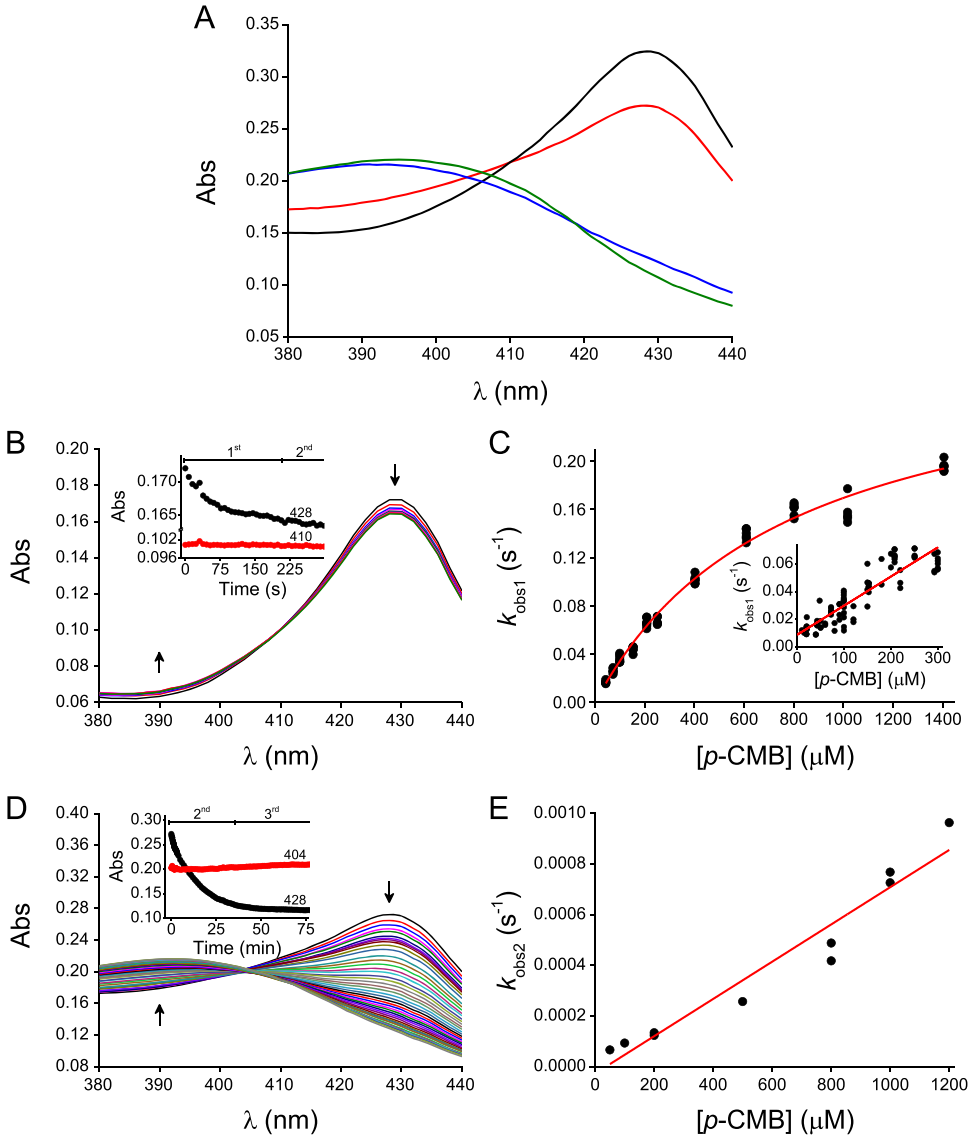

Figure 1. Reaction of Fe(III)-CBS with *p*-CMB. (A) UV−visible absorption spectra of Fe(III)-CBS (4 μM) mixed with *p*-CMB (1 mM) in Tris−HCl buffer (0.1 M, pH 7.4) at 25 °C. Spectra correspond to CBS before addition of *p*-CMB (black) and to the products of the first phase, recorded immediately after mixing (red), of the second phase, recorded after 35 min (blue), and of the third phase, recorded after 12 h (green). (B) Spectral changes during the first phase of the reaction between CBS (2 μM) and *p*-CMB (100 μM), registered every 23 s over the first 210 s of the reaction. The arrows indicate the direction of the absorbance changes over time. The maximum remained at 428 nm, and there was an isosbestic point at 410 nm. Inset: time courses at 410 and 428 nm. (C) Kinetics of the first phase. Exponential plus straight line functions were fitted to stopped-flow kinetic traces at 430 nm of Fe(III)-CBS (4 μM) and *p*-CMB (72−1017 μM) over 10 half-lives. The obtained observed rate constants (k_{obs1}) showed a hyperbolic dependence on *p*-CMB concentration with values of 0.301 ± 0.008 s^{-1} for the horizontal asymptote and (7.8 ± 0.4) × 10^{-4} M for the concentration of *p*-CMB at which k_{obs1} was half-maximal (parameters ± errors of the fit, R^2 = 0.987). Inset: dependence of the observed rate constants on relatively low *p*-CMB concentrations (0 to 300 μM). The *y*-intercept had a value of (9 ± 2) × 10^{-3} s^{-1} (parameter ± error of the fit, R^2 = 0.816). (D) Spectral changes associated with the second phase of the reaction between CBS (4 μM) and *p*-CMB (1 mM). Spectra were recorded every 21.5 s over the first 4 min and every 1 min until 35 min. The product had an absorption maximum at 391 nm, and there was an isosbestic point at 404 nm. Inset: time courses at 404 and 428 nm. (E) Kinetics of the second phase. Exponential plus straight line functions were fitted to the observed traces at 430 nm for the reaction between Fe(III)-CBS (2 μM) and *p*-CMB over 4−10 half-lives. k_{obs2} showed a linear dependence on *p*-CMB concentration with a slope of 0.74 ± 0.06 M^{-1} s^{-1} (parameter ± error of the fit, R^2 = 0.935).

ferricyanide reduction (ε_{420} = 1020 M^{-1} cm^{-1}) assuming a 2:1 (ferricyanide:dithionite) stoichiometry.[48] The desired concentration of *p*-CMB was achieved by diluting a stock solution of *p*-HMB in Tris−HCl buffer (0.1 M, pH 7.4) under anoxic conditions. In order to avoid oxygen contamination, 40 μM protocatechuate and 1 μM protocatechuate 3,4-dioxygenase[65] were included in the Fe(II)-CBS and *p*-CMB solutions. Kinetic studies using Fe(II)-CBS were performed using a Hi-Tech Scientific SF-61DX stopped-flow spectrophotometer in the photodiode array mode flushed with buffer containing the protocatechuate-protocatechuate 3,4-dioxygenase mixture. Data were analyzed with the Kinetic Studio software.

Separation of Heme from the Protein after Exposure to Mercury Compounds. Fe(III)-CBS (11 μM) was exposed to 100 μM $HgCl_2$ or *p*-CMB for 48 h in Tris−HCl buffer (0.1 M, pH 7.4) at 4 °C. Samples were then filtered using Corning Spin-X UF 500 concentrators (MWCO 10 kDa) in two 15 min cycles at 10,000 *g* and 4 °C. The UV−visible spectra of the

https://dx.doi.org/10.1021/acsomega.0c05475
ACS Omega 2021, 6, 2192−2205

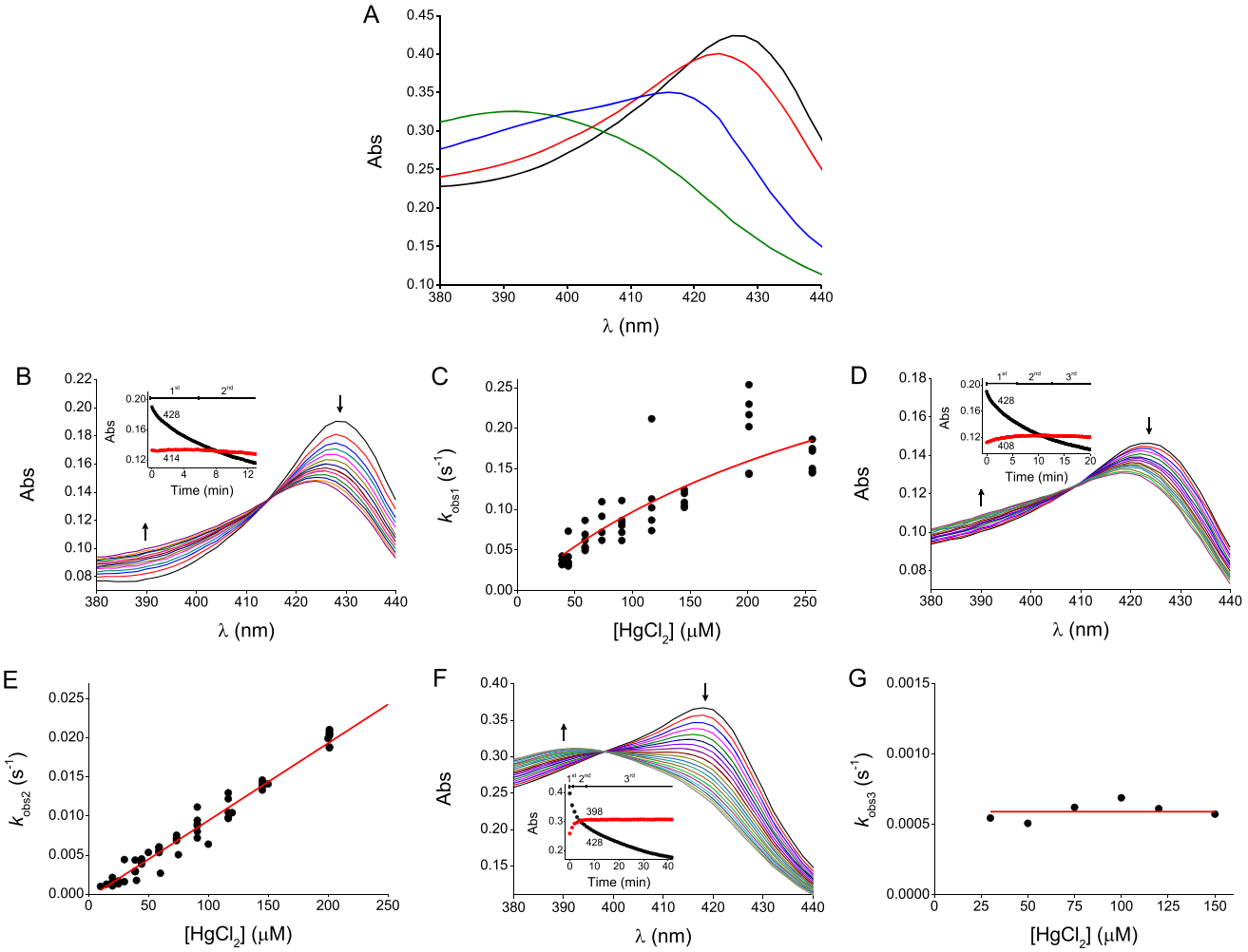

Figure 2. Reaction of Fe(III)-CBS with $HgCl_2$. (A) UV−visible absorption spectra of Fe(III)-CBS (5 μM) mixed with $HgCl_2$ (100 μM) in Tris−HCl buffer (0.1 M, pH 7.4) at 25 °C. The shown spectra were recorded immediately after mixing (black) and after 58 s (red), 11.6 min (blue), and 1.3 h (green) of the reaction, corresponding to the products of the first, second, and third phases, respectively. (B) Spectral changes during the first phase of the reaction between CBS (2 μM) and $HgCl_2$ (20 μM), recorded every 28 s over the first 5.8 min of the reaction. The arrows indicate the direction of the absorbance changes over time. The absorption maximum changed from 428 to 424 nm with an isosbestic point at 414 nm. Inset: time courses at 414 and 428 nm. (C) Kinetic analysis of the first phase. Double exponential plus straight line functions were fitted to stopped-flow kinetic traces at 430 nm of the first phase of the reaction between Fe(III)-CBS (4 μM) and $HgCl_2$ ($\leq$256 μM). In the traces with [$HgCl_2$] < 90 μM, a rapid decrease at 428 nm was observed, and so, the first 10 s were excluded from the fit. The observed rate constants showed a hyperbolic dependence on $HgCl_2$ concentration with a value of 0.4 ± 0.1 s^{-1} for the horizontal asymptote and (4 ± 1) × 10^{-4} M for the concentration of $HgCl_2$ at which k_{obs1} is half-maximal (parameters ± errors of the fit, R^2 = 0.728). The extrapolation of the initial straight line yielded a *y*-intercept of (6.7 ± 0.3) × 10^{-3} s^{-1}. (D) Spectral variations during the second phase of the reaction between CBS (2 μM) and $HgCl_2$ (20 μM), recorded every 28 s between 5.9 and 12.6 min of the reaction. The absorption maximum shifted from 424 to 418 nm with an isosbestic point at 408 nm. Inset: time courses at 408 and 428 nm. (E) Kinetic analysis of the second phase. Double exponential or double exponential plus straight line functions were fitted to kinetic traces at 430 nm of the reaction between Fe(III)-CBS (2, 4, or 5 μM) and $HgCl_2$ (20−256 μM). k_{obs2} showed a linear dependence on $HgCl_2$ concentration with a slope of 99 ± 2 M^{-1} s^{-1} (parameter ± error of the fit, R^2 = 0.979). (F) Spectral changes of the third phase of the reaction between CBS (5 μM) and $HgCl_2$ (120 μM). Spectra recorded every 116 s between 6.8 and 42 min of the reaction. The absorption maximum at 418 shifted to 390 nm with an isosbestic point at 398 nm. Inset: time courses at 398 and 428 nm registered every 58 s. (G) Kinetic analysis of the third phase. Double exponential or double exponential plus straight line functions were fitted to kinetic traces at 430 nm of the reaction between Fe(III)-CBS (3 or 5 μM) and $HgCl_2$ (30−150 μM). The smaller k_{obs}s of the fits were independent of $HgCl_2$ concentration yielding a constant of (5.9 ± 0.6) × 10^{-4} s^{-1} (mean ± S.D.).

retentate and filtrate fractions were recorded with a Varian Cary 50 spectrophotometer.

Activity Measurements. Mixtures of 5.7 μM Fe(III)-CBS and 100 μM $HgCl_2$ or *p*-CMB in Tris−HCl buffer (0.1 M, pH 7.4) were incubated at 4 °C. After 0.5 or 72 h, the mixtures were filtered and washed using Corning Spin-X UF 500 concentrators (MWCO 10 kDa) to remove the free mercury compounds. The UV−visible absorption spectrum of the protein was recorded, and its activity was measured by the ninhydrin method.[61] The concentration of CBS was calculated from the absorbance at 280 nm using the extinction coefficient for untreated protein (ε_{280} = 92,200 M^{-1} cm^{-1}). The specific activity of cystathionine formation was expressed as μmol min^{-1} mg^{-1} (37 °C).

Quantum Mechanics (QM) Energy Minimization. In order to investigate the effect of the mercury compounds on the Fe−S_{Cys} bond, QM energy minimization in vacuum was performed with Gaussian03.[66] These calculations were done

https://dx.doi.org/10.1021/acsomega.0c05475
ACS Omega 2021, 6, 2192−2205

using the generalized gradient approximation functional proposed by Perdew, Burke, and Ernzerhof (PBE),[67] using 6-31G(d,p) basis sets for all non-mercury atoms and SBKJC-VDZ (VDZ Valence Double Zeta with ECP) basis set for the mercury atom. The structural model of the heme binding site consisted of a heme group (excluding side chains), an imidazole (representing His65), a methylthiolate (representing Cys52), and the mercury compound. In total, four models were constructed, in which the mercury compound varied between *p*-CMB, *p*-mercuribenzoic acid (*p*-MB, without chloride or hydroxyl ligands), and $HgCl_2$. For this last compound, models with one or two $HgCl_2$ molecules were calculated. Mercury compounds were located in proximity to the thiolate and allowed to freely optimize their position.

Hybrid Quantum Mechanics/Molecular Mechanics (QM/MM) Calculation. Hybrid QM/MM geometry optimizations were performed with a conjugate gradient algorithm at the density functional theory (DFT) level with the SIESTA code and QM/MM implementation.[68,69] The QM subsystems were treated at the DFT level as described above, whereas the classical subsystems were treated using the Amber99SB force field parametrization.[70] Only the residues located within 10 Å from the iron center were allowed to move freely. The frontier between the QM and MM portions of the system was treated with the scaled position link atom method.[71] The initial structure used corresponded to the crystal structure of full-length human CBS (PDB id: 4PCU).[72] The QM subsystems consisted of the heme group (without side chains), the axial ligands (the thiolate of Cys52 and the imidazole ring of His65), and the mercury compound. The rest of the protein and the water molecules were treated classically. A similar approach has been applied previously to several heme proteins.[73−76] To construct the initial structures for the QM/MM calculations that include the protein and the mercury compounds, we aligned the heme group and the axial ligands, located the mercury compounds according to the result of the isolated systems, and allowed them to freely optimize their position. Using this strategy, we found two possible initial poses for *p*-CMB and *p*-MB, which were called "in" and "out", one with the mercury compound partially inside the protein matrix ("in" conformation) and the other where the mercury compound was located in the solvent ("out" conformation).

RESULTS AND DISCUSSION

Kinetics of the Reaction of Fe(III)-CBS with *p*-CMB. Exposure of Fe(III)-CBS to an excess of *p*-CMB under pseudo-first-order conditions led to the disappearance of the peak at 428 nm and to the formation of a species with absorbance at 395 nm over a 12 h time course. No single isosbestic point was identified, suggesting that the overall process was multiphasic (Figure 1A). The reaction occurred in three kinetic phases, which are described below.

In the first phase, the absorption spectrum changes were small. On a timescale of 10−100 s, depending on the concentration of *p*-CMB, the absorbance at 428 nm decreased while that at 390 nm increased, with an isosbestic point at 410 nm (Figure 1B). Although the intensity of the 428 nm peak decreased, the λ_{max} was unchanged, indicating that heme remained six-coordinate. Exponential plus straight line functions were fitted to the reaction time courses over 10 half-lives. Both the exponential rate constant for the first phase (k_{obs1}) (Figure 1C) and the amplitude (not shown) showed a hyperbolic dependence on *p*-CMB concentration. From the plot of k_{obs1} *versus* *p*-CMB concentration, a limiting value at infinite *p*-CMB concentration of 0.301 ± 0.008 s^{-1} was obtained, while the concentration of *p*-CMB at which k_{obs1} was half-maximal was $(7.8 \pm 0.4) \times 10^{-4}$ M (Figure 1C). To more accurately assess the *y*-axis intercept, the experiment was repeated at lower *p*-CMB concentrations and a value of $(9 \pm 2) \times 10^{-3}$ s^{-1} was obtained for the intercept (Figure 1C inset), suggesting that the first phase of the interaction between Fe(III)-CBS and *p*-CMB was reversible.

The second phase of the reaction between Fe(III)-CBS and *p*-CMB occurred on a timescale of minutes to hours, depending on the concentration of *p*-CMB. This phase was associated with the largest spectral change; the peak at 428 nm shifted to 391 nm with an isosbestic point at 404 nm (Figure 1D). The shift to 391 nm is indicative of the formation of a five-coordinate species.[21,77−79] Exponential plus straight line functions were fitted to the time courses, and values of k_{obs2} were obtained at different *p*-CMB concentrations. The plot of k_{obs2} *versus* *p*-CMB concentration was linear, suggesting that *p*-CMB participated directly in the reaction with a second-order rate constant of 0.74 ± 0.06 M^{-1} s^{-1} (Figure 1E).

In the third phase, the maximum at 391 nm shifted to 395 nm (Figure 1A), consistent with the continued presence of a five-coordinate species on an even longer timescale. The kinetics of this slow third phase was not studied further.

Kinetics of the Reaction of Fe(III)-CBS with $HgCl_2$. When Fe(III)-CBS was mixed with excess $HgCl_2$, the absorption spectrum peak shifted from 428 to 390 nm in a multiphasic process without a single isosbestic point (Figure 2A). This reaction occurred in three main phases that are described below.

The first phase occurred on a timescale of 10−100 s. The peak at 428 shifted to 424 nm and the absorbance around 390 nm increased, with an isosbestic point at 414 nm (Figure 2B). The maximum at 424 nm suggested that heme remained six-coordinate.[77,80,81] Stopped-flow spectroscopic analysis of the kinetics of this phase showed a hyperbolic dependence on the observed rate constant on $HgCl_2$ concentration, with values of 0.4 ± 0.1 s^{-1} for the horizontal asymptote and $(4 \pm 1) \times 10^{-4}$ M for the concentration of $HgCl_2$ at which k_{obs1} is half-maximal (Figure 2C). The *y*-intercept was obtained using the data points below 60 μM $HgCl_2$ and had a value of $(6.7 \pm 0.3) \times 10^{-3}$ s^{-1}. The amplitude for the first phase also showed a hyperbolic dependence on $HgCl_2$ concentration (not shown). It is worth noting that in experiments with low $HgCl_2$ concentration (<90 μM), an initial rapid decrease in absorbance at 428 nm was observed (k_{obs} of ~0.2 s^{-1}), with no other spectral changes. The low amplitude of this change (~0.01) made its characterization difficult.

In the second phase of the reaction between $HgCl_2$ and Fe(III)-CBS, the peak shifted from 424 to 418 nm characteristic of a six-coordinate heme with two neutral ligands,[78,82−84] on a timescale of minutes. The absorbance at 390 nm continued to increase, with an isosbestic point at 408 nm (Figure 2D). k_{obs2} showed a linear dependence on $HgCl_2$ concentration and yielded a second-order rate constant of 99 ± 2 M^{-1} s^{-1} (Figure 2E).

The third phase of the reaction resulted in a species with a maximum absorbance at 390 nm, indicative of a five-coordinate species[21,77−79] and an isosbestic point at 398 nm (Figure 2F). The observed rate constants, $(5.9 \pm 0.6) \times 10^{-4}$ s^{-1}, were independent of $HgCl_2$ concentration (Figure 2G).

https://dx.doi.org/10.1021/acsomega.0c05475
ACS Omega 2021, 6, 2192−2205

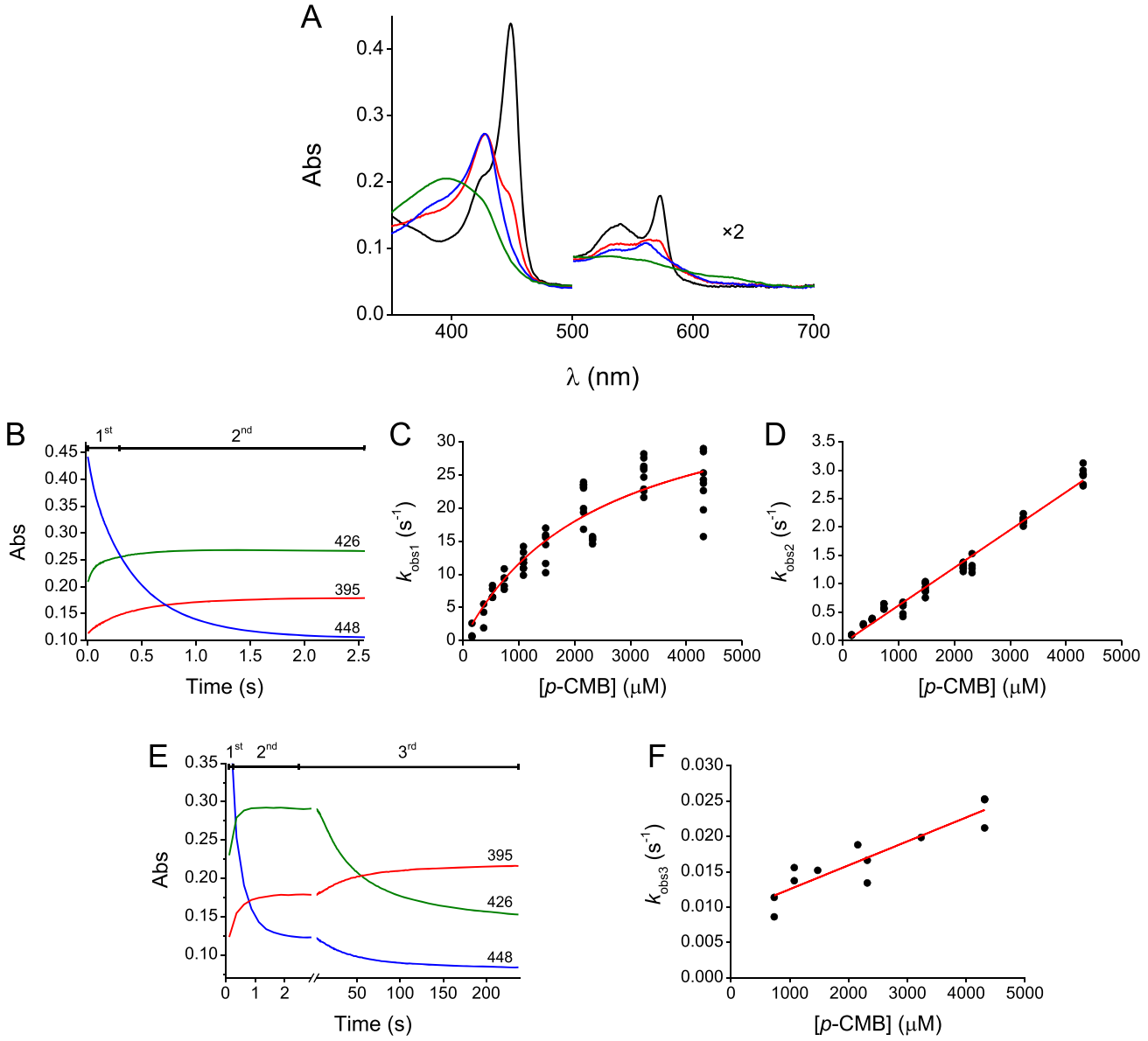

Figure 3. Reaction of Fe(II)-CBS with *p*-CMB. (A) UV−visible absorption spectra of Fe(II)-CBS (4 μM) mixed with *p*-CMB (4.3 mM) in Tris−HCl buffer (0.1 M, pH 7.4) under anoxic conditions at 25 °C, registered at 0.05 (black), 0.65 (red), 3.05 (blue), and 95 s (green). (B) Time courses for absorbance changes at 448, 426, and 395 nm obtained from a shorter register. (C) Kinetic analysis of the first phase. The k_{obs1} obtained from the double exponential function fit to the increase in absorption at 426 nm showed a hyperbolic dependence on the concentration of *p*-CMB and yielded a value of 40 ± 4 s^{-1} for the horizontal asymptote and (2.5 ± 0.5) × 10^{-3} M for the concentration of *p*-CMB at which k_{obs1} is half-maximal (parameters ± errors of the fit, R^2 = 0.853). (D) Kinetic analysis of the second phase. The k_{obs2} obtained from the double exponential fit to the increase in absorption at 426 nm showed a linear dependence on *p*-CMB concentration with a slope of (6.7 ± 0.1) × 10^2 M^{-1} s^{-1} (parameter ± error of the fit, R^2 = 0.981). (E) Longer time courses obtained under the same conditions used in the experiment shown in panel (A). (F) Kinetic analysis of the third phase. A linear function was fitted to the k_{obs3} obtained from time courses at 395 nm (single exponential fits after the end of the second phase). The slope was 3.4 ± 0.5 M^{-1} s^{-1}, and the *y*-intercept was (9 ± 1) × 10^{-3} s^{-1} (parameters ± errors of the fit, R^2 = 0.819).

Kinetics of the Reaction of Fe(II)-CBS with *p*-CMB. Exposure of Fe(II)-CBS to *p*-CMB under anoxic conditions resulted in rapid changes in the heme absorbance spectrum. The maximum shifted from 448 to 395 nm in a multiphasic process consisting of four phases (Figure 3A).

During the first 1−10 s of the reaction, depending on the concentration of *p*-CMB, a fast decay in the absorbance at 448 nm was observed while a species with a peak at 426 nm was formed, with no clear isosbestic point (Figure 3B). The intermediate at 426 nm has been observed previously[21,38] and cannot be mistaken with the oxidized form of CBS since the spectral change of the heme-thiolate Soret peak coincides with decreases at 572 and 539 nm to produce new blue-shifted peaks at 559 and 530 nm, absent in the ferric form of the enzyme. A 426 nm intermediate was reported[51] during heat treatment of Fe(II)-CBS at pH 9.0 and hypothesized to result from the exchange of the thiolate ligand with a neutral ligand. The initial rapid absorbance changes at 448 and 426 nm were biphasic. The observed rate constants obtained from double exponential function fits showed a hyperbolic (k_{obs1}) and a linear (k_{obs2}) dependence on the concentration of *p*-CMB (Figure 3C,D) for the first and second phases of the reaction, respectively. From the plots of the observed rate constants as a function of *p*-CMB concentration, a maximal k_{obs1} of (40 ± 4)

https://dx.doi.org/10.1021/acsomega.0c05475
ACS Omega 2021, 6, 2192−2205

Table 1. Reactions between CBS and Mercury Compounds[a]

reaction	phase	k_{obs} *versus* mercury compound	λ_{max} of the product (nm)	isosbestic point (nm)
Fe(III)-CBS (428 nm) and *p*-CMB	1	hyperbolic: $k_{obs\ max}$ = 0.301 ± 0.008 s^{-1}; [*p*-CMB] at (1/2)$k_{obs\ max}$ = (7.8 ± 0.4) × 10^{-4} M; *y*-intercept = (9 ± 2) × 10^{-3} s^{-1}	428	410
	2	linear: slope = 0.74 ± 0.06 M^{-1} s^{-1}	391	404
	3	N.D.	395	N.D.
Fe(III)-CBS (428 nm) and $HgCl_2$	1	hyperbolic: $k_{obs\ max}$ = 0.4 ± 0.1 s^{-1}; [$HgCl_2$] at (1/2)$k_{obs\ max}$ = (4 ± 1) × 10^{-4} M; *y*-intercept = (6.7 ± 0.3) × 10^{-3} s^{-1}	424	414
	2	linear: slope = 99 ± 2 M^{-1} s^{-1}	418	408
	3	constant: *k* = (5.9 ± 0.6) × 10^{-4} s^{-1}	390	398
Fe(II)-CBS (448 nm) and *p*-CMB	1	hyperbolic: $k_{obs\ max}$ = 40 ± 4 s^{-1}; [*p*-CMB] at (1/2) $k_{obs\ max}$ = (2.5 ± 0.5) × 10^{-3} M	N.D.	N.D.
	2	linear: slope = (6.7 ± 0.1) × 10^2 M^{-1} s^{-1}	426	N.D.
	3	linear: slope = 3.4 ± 0.5 M^{-1} s^{-1}; *y*-intercept (9 ± 1) × 10^{-3} s^{-1}	395	N.D.
	4	k_{obs} ~1 × 10^{-3} s^{-1}	N.D.	N.D.

[a]Experiments were performed at 25 °C in Tris−HCl buffer (0.1 M, pH 7.4). N.D., not determined.

s^{-1} and a *p*-CMB concentration at half-maximal k_{obs} of (2.5 ± 0.5) × 10^{-3} M were determined for the first phase; a second-order rate constant of (6.7 ± 0.1) × 10^2 M^{-1} s^{-1} was determined for the second phase.

In the third phase, the 426 nm intermediate shifted to a 395 nm broad band typical of a five-coordinate heme lacking thiolate ligation, on a timescale of minutes (Figure 3E), with a k_{obs3} in the order of 0.01−0.02 s^{-1} and a weak dependence on *p*-CMB concentration (Figure 3F). This third phase was followed by a slower phase with a half-life of ~10 min that was not studied further.

Analysis of the Kinetics of the Reactions between Fe(III)-CBS and Fe(II)-CBS with Mercury Compounds. The results of our kinetic studies are summarized in Table 1. The reactions of Fe(III)-CBS with *p*-CMB or $HgCl_2$ were multiphasic. In the first phase of both reactions, the observed rate constants increased hyperbolically with concentration of the mercury compound. Hence, the first phase involves at least two steps and can be analyzed in terms of the two possible models for the binding of an enzyme to a ligand, the conformational selection and the induced fit models.[85,86] In the conformational selection model, the enzyme exists minimally in two conformations of which only one binds the ligand (*i.e.*, the mercury compound). In the induced fit model, the ligand binds to the enzyme and the initial complex undergoes a conformational change. The species formed with *p*-CMB and $HgCl_2$ in the first phase have different absorbance peaks (428 and 424 nm, respectively); however, we assign both as six-coordinate heme species.

Using the conformational selection model as a framework (eq 1), we postulate for the initial reaction that six-coordinate Fe(III)-CBS (*A*) can transform reversibly into a species with a weaker cysteine ligand (*B*) with forward and reverse rate constants k_r and k_{-r}. Either *p*-CMB or $HgCl_2$ (denoted as *L*) binds only to *B* with an apparent forward rate constant $k_{on}[L]$ and a reverse rate constant k_{off}, yielding a six-coordinate heme species (*C*) with His65 and Cys52 ligands, in which the cysteine is also coordinated to mercury. The proposed difference between the *A* and *B* conformers is the strength of the Fe−S_{Cys52} bond or, alternatively, disruption of the interaction between the thiolate of Cys52 and Arg266 or Trp54.

$$A \underset{k_{-r}}{\overset{k_r}{\rightleftharpoons}} B \underset{k_{off}}{\overset{k_{on}[L]}{\rightleftharpoons}} C \quad (1)$$

Considering steady state for *B*, we obtain eq 2.

$$k_{obs} = \frac{k_r k_{on}[L] + k_r k_{off} + k_{-r} k_{off}}{k_{on}[L] + k_{-r} + k_{off}} \quad (2)$$

Assuming that $k_{off} \ll k_{-r}$ and $k_{off} \ll k_r$ (*i.e.*, the dissociation of the mercury compound is slow, slower than the conversion of *B* to *A* and of *A* to *B*) and that $k_r \ll k_{-r}$ (*i.e.*, the conversion of *A* to *B* is slower than that of *B* to *A*), the rate constants can be estimated from plots of k_{obs1} *versus* the concentration of the mercury compound. The values for k_r obtained from the limiting value for k_{obs} at infinite concentrations of *p*-CMB and $HgCl_2$ are similar, 0.301 ± 0.008 and 0.4 ± 0.1 s^{-1}, respectively, consistent with the independence of this rate constant on [*L*], the concentration of the mercury compound. The rate constants for the dissociation of the mercury compound (k_{off}) were also similar for *p*-CMB ((9 ± 2) × 10^{-3} s^{-1}) and $HgCl_2$ ((6.7 ± 0.3) × 10^{-3} s^{-1}). Values of k_{-r}/k_{on} were (7.8 ± 0.4) × 10^{-4} and (4 ± 1) × 10^{-4} M for *p*-CMB and $HgCl_2$, respectively, suggesting that the rate constant for binding to *B* (k_{on}) is ~2-fold higher for the smaller $HgCl_2$ than for the larger *p*-CMB mercury compound.

Alternatively, using the induced fit model as a framework (eq 3), we postulate that CBS is initially six-coordinate (*A*) and that the binding of either *p*-CMB or $HgCl_2$ (*L*) triggers the formation of an initial enzyme−ligand complex (*B*) with an apparent forward rate constant $k_{on}[L]$ and a reverse rate constant k_{off}. Intermediate *B* undergoes a conformational change to *C* with forward and reverse rate constants k_r and k_{-r}, respectively. The species *C* is proposed to remain six-coordinate and to have His65 and Cys52, also bound to mercury, as ligands.

$$A \underset{k_{off}}{\overset{k_{on}[L]}{\rightleftharpoons}} B \underset{k_{-r}}{\overset{k_r}{\rightleftharpoons}} C \quad (3)$$

Considering a rapid equilibrium for ligand binding followed by a slow conformational change step, we obtain eq 4.

$$k_{obs} = \frac{k_r[L]}{K_d + [L]} + k_{-r} \quad (4)$$

Assuming $k_{-r} \ll k_r$, from the plots of k_{obs1} *versus* the concentration of the mercury compound, we can estimate the values for k_{-r} ((9 ± 2) × 10^{-3} s^{-1} for *p*-CMB and (6.7 ± 0.3) × 10^{-3} s^{-1} for $HgCl_2$) and for k_r (0.301 ± 0.008 s^{-1} for *p*-CMB and 0.4 ± 0.1 s^{-1} for $HgCl_2$). In this model, we assign k_r as the rate constant for the weakening of the Fe−S_{Cys52} bond.

https://dx.doi.org/10.1021/acsomega.0c05475
ACS Omega 2021, 6, 2192−2205

To sum up, either model can explain the experimental data, *i.e.*, the hyperbolic first phase for the reaction between Fe(III)-CBS and *p*-CMB or $HgCl_2$. In both models, the product of the first phase of the reaction is a six-coordinate heme, which, we propose, retains its histidine and cysteine ligands, with the latter additionally coordinating to mercury. While the species formed with *p*-CMB and $HgCl_2$ show differences in the absorption spectra (428 and 424 nm maxima, respectively), these differences could be due to differences in the size and/or charge of *p*-CMB and $HgCl_2$.

In the second phase of the reaction between Fe(III)-CBS and the mercury compounds, k_{obs2} increased linearly with concentration. This is interpreted as evidence that a second mole of the mercury compound bound to the thiolate of the cysteine in a single step. The second-order rate constant was ~130-fold faster for $HgCl_2$ than for *p*-CMB, 99 ± 2 *versus* 0.74 ± 0.06 M^{-1} s^{-1}, respectively. The species with an absorption maximum at 391 nm that is formed in the reaction with *p*-CMB is assigned as a five-coordinate species.[21,77−79] Since *p*-CMB is bulky, it is likely to constrain coordination of Cys52 to the heme iron and to two molecules of *p*-CMB. Instead, binding of a second molecule of *p*-CMB could trigger dissociation of the thiolate ligand resulting in a five-coordinate heme. In the reaction with $HgCl_2$, the resulting species has a peak at 418 nm, consistent with a six-coordinate species. The steric constraints with $HgCl_2$ are lower than with *p*-CMB, and we propose that the thiolate ligand coordinates two mercury ions and the heme iron, explaining the presence of a six-coordinate heme. In this regard, there is precedent for the binding of thiolates to more than one mercury compound. Two-to-one complexes of methylmercury and glutathione or *N*-acetylcysteine have been reported, as well as complexes of cysteine and Hg(II) with bridging sulfurs.[87−89]

In the third phase of the reaction of Fe(III)-CBS with $HgCl_2$, a species with an absorption maximum at 390 nm is formed, consistent with a five-coordinate heme lacking the thiolate ligand, with an apparent rate constant of 6×10^{-4} s^{-1}. Interestingly, addition of thiols to CBS treated with $HgCl_2$ resulted in a red shift in the spectrum to 424 nm rather than the starting 428 nm Soret peak.[38] Exogenous thiols would react with some mercury compounds reversing the second and third phases, but not the first. Thus, the cysteine probably remained coordinated to 1 equiv. of mercury under the reported conditions; otherwise, a peak at 428 nm would have been observed.

In the case of the reaction of Fe(II)-CBS toward *p*-CMB, the hyperbolic behavior of the k_{obs1} obtained in the first phase can also be explained by either the conformational selection or the induced fit models. The ferrous heme coordination is labile as compared to the ferric form and is consistent with the ~100-fold higher k_{obs1} for Fe(II)-CBS (40 ± 4 s^{-1}) than for Fe(III)-CBS (0.3−0.4 ± 0.1 s^{-1}). In addition, the second phase exhibited a second-order rate constant of $(6.7 \pm 0.1) \times 10^2$ M^{-1} s^{-1}, which is significantly higher than the values for Fe(III)-CBS of 0.74 ± 0.06 M^{-1} s^{-1} with *p*-CMB and 99 ± 2 M^{-1} s^{-1} with $HgCl_2$. These phases led to the formation of a six-coordinate species that then decayed to a five-coordinate one in the third phase. The rate constant for the third phase was 0.01−0.02 s^{-1}, which is comparable in value to the limiting rate constant for binding of CO to Fe(II)-CBS, *i.e.*, 0.003−0.017 s^{-1}[41,42,45,53] and is assumed to represent the dissociation of the thiolate ligand in Fe(II)-CBS. However, in our experiments, the dissociated thiolate would be coordinated to mercury.

Finally, it is important to consider that some of the changes observed, particularly those at long time points, could be affected by interactions of the mercury compounds with other residues on CBS, which could potentially lead to alterations in the heme environment.

QM and QM/MM Calculations of the Intermediate States for the Reactions between CBS and Mercury Compounds. To further characterize the reaction between mercury compounds and Fe(II)- or Fe(III)-CBS, we performed calculations in model systems and in the complete protein. The main goal was to detect possible intermediate complexes that could explain the kinetic behavior observed. We also intended to examine how the presence of the mercury compounds affected the Fe−S bond. For this purpose, we first generated different model systems and then added the mercury compounds inside the protein heme cavity.

Model systems included a heme group, two axial ligands (methylthiolate representing the bound cysteine and imidazole for the bound histidine), and the different mercury compounds ($HgCl_2$, *p*-CMB, and *p*-MB, described in the Materials and Methods section). As expected, the Fe−S distance was shorter for the ferric state than for the ferrous state, and low-spin states showed shorter Fe−S distances than high-spin states both in the ferric and ferrous oxidation states (Table 2). The presence of mercury compounds increased the Fe−S distance in all cases. In the low-spin states, for both oxidation states of iron, the increment in the Fe−S bond distance was very small, while in the high-spin states, we observed larger variations. In the case of $HgCl_2$, the results indicated that the thiolate could interact with two molecules of $HgCl_2$ at the same time, with a slightly larger Hg−S distance than in the case with only one molecule, but producing in most cases a larger elongation of the Fe−S bond. Comparing the *p*-CMB and the *p*-MB complexes, the Hg−S distance was shorter in the model with *p*-MB, while the Fe−S bond distance was larger, indicating that *p*-MB, without a coordinated chloride, was more effective at pulling away the thiolate ligand from the heme iron. Of note, the chloride ions are labile and likely to be exchanged by other ligands including sulfur ligands.

Table 2. Relevant Distances in the Isolated Model Systems with the Different Mercury Compounds[a]

	Fe(II)		Fe(III)	
	low spin	high spin	low spin	high spin
Fe−S distance				
without the Hg compound	2.32	2.37	2.20	2.34
1 $HgCl_2$	2.34	2.62	2.25	2.47
2 $HgCl_2$	2.33	3.07	2.29	2.56
p-CMB	2.36	2.60	2.24	2.61
p-MB	2.34	2.81	2.32	2.73
Hg−S distance				
1 $HgCl_2$	2.52	2.50	2.71	2.64
2 $HgCl_2$[b]	2.64	2.589	2.85	2.77
p-CMB	2.56	2.52	3.11	2.87
p-MB	2.48	2.46	2.47	2.44

[a]Results are shown for the Fe(II) and Fe(III) states in low- and high-spin states. The Fe(II) states correspond to singlet and triplet spin states, while the Fe(III) states correspond to doublet and sextuplet spin states. Distances are given in Å. [b]Mean distance to both Hg atoms.

https://dx.doi.org/10.1021/acsomega.0c05475
ACS Omega 2021, 6, 2192−2205

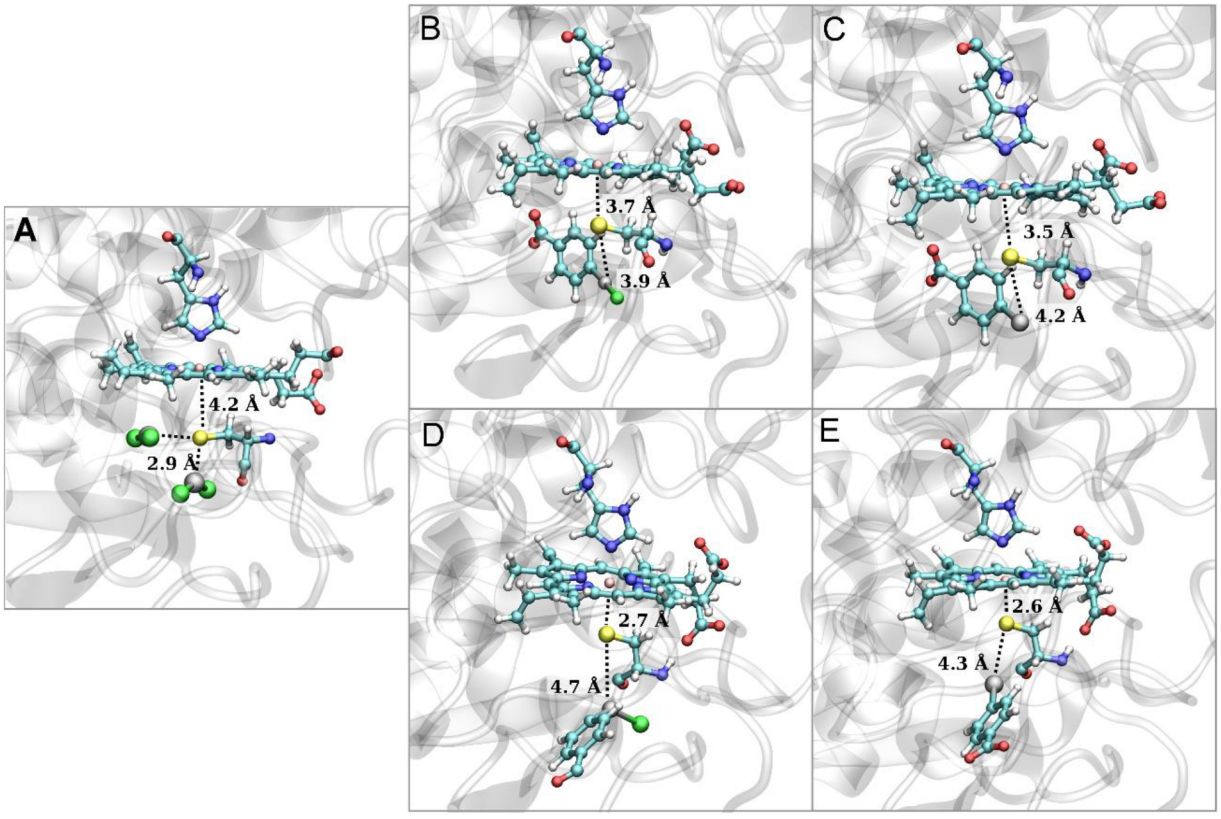

Figure 4. Structures of Fe(III)-CBS with the mercury compounds. (A) Two $HgCl_2$ molecules, (B) *p*-CMB "in" conformation, (C) *p*-MB "in" conformation, (D) *p*-CMB "out" conformation, and (E) *p*-MB "out" conformation. All the structures correspond to the high-spin ferric state.

Apart from the QM calculations in isolated model systems, QM/MM calculations were performed in order to determine plausible structures for the complexes between CBS and the different mercury compounds. We were able to obtain stable structures of CBS with the mercury compounds (Figure 4). Although the Hg−S_{Cys52} distances were larger than in the isolated model systems, we still observed an elongation of the Fe−S_{Cys52} bond (Table 3). Of note, the Fe−S_{Cys52} distance computed for low-spin Fe(III)-CBS in the absence of mercury compounds was consistent with previous experimental and theoretical determinations.[90] For *p*-CMB and *p*-MB, two conformations were studied, one with the mercury compound partially inside the protein ("in") and the other one with the mercury compound in the solvent ("out"). The "in" conformation was more effective in weakening the Fe−S_{Cys52} bond, as evidenced in the larger Fe−S_{Cys52} distances and the smaller Hg−S_{Cys52} distances observed in the optimized structure, compared to the "out" conformation. In contrast to what was observed in the isolated models, in the complex with *p*-CMB, the increase in the Fe−S_{Cys52} distance was larger than with *p*-MB (in both conformations), where the cysteine remained close to the iron. This is possibly due to the larger steric hindrance of *p*-CMB than of *p*-MB.

Altogether, the results from the calculations indicate that it is possible to obtain stable complexes with CBS and the different mercury compounds considered in this work. Coordination by mercury pulls the Cys52 ligand away from the iron ion, but the cysteine can remain within coordination distance, providing evidence for the proposed intermediate states with the cysteine still close to the iron but also bound to the mercury compounds. The computational results also provide evidence for the possibility of interaction of two mercury compounds with the heme-thiolate, as suggested from the kinetic results with $HgCl_2$.

Table 3. Relevant Distances in CBS with the Different Mercury Compounds[a]

	Fe(II)		Fe(III)	
	low spin	high spin	low spin	high spin
Fe−S_{Cys52} distance				
without the Hg compound	2.32	2.37	2.20	2.34
2 $HgCl_2$	4.11	3.87	3.76	4.16
"in" *p*-CMB	3.54	3.51	2.49	3.69
"in" *p*-MB	3.83	3.69	3.87	3.47
"out" *p*-CMB	2.53	2.83	2.38	2.70
"out" *p*-MB	2.42	2.59	2.39	2.58
Hg−S_{Cys52} distance				
2 $HgCl_2$[b]	2.87	3.26	2.89	2.80
"in" *p*-CMB	4.01	4.00	4.83	3.93
"in" *p*-MB	3.01	3.84	2.94	4.17
"out" *p*-CMB	4.74	4.18	5.20	4.70
"out" *p*-MB	4.37	4.14	4.47	4.25

[a]Results are shown for Fe(II)- and Fe(III)-CBS in low- and high-spin states. The Fe(II) states correspond to singlet and triplet spin states, while the Fe(III) states correspond to doublet and sextuplet spin states. The term "in" corresponds to the conformation where the mercury compound is partially inside the protein matrix, while "out" corresponds to the conformation where the mercury compound is located in the solvent. Distances are given in Å. [b]Mean distance to both Hg atoms.

Separation of Heme from the Protein. To determine if heme is released from the protein after exposure to mercury

https://dx.doi.org/10.1021/acsomega.0c05475
ACS Omega 2021, 6, 2192−2205

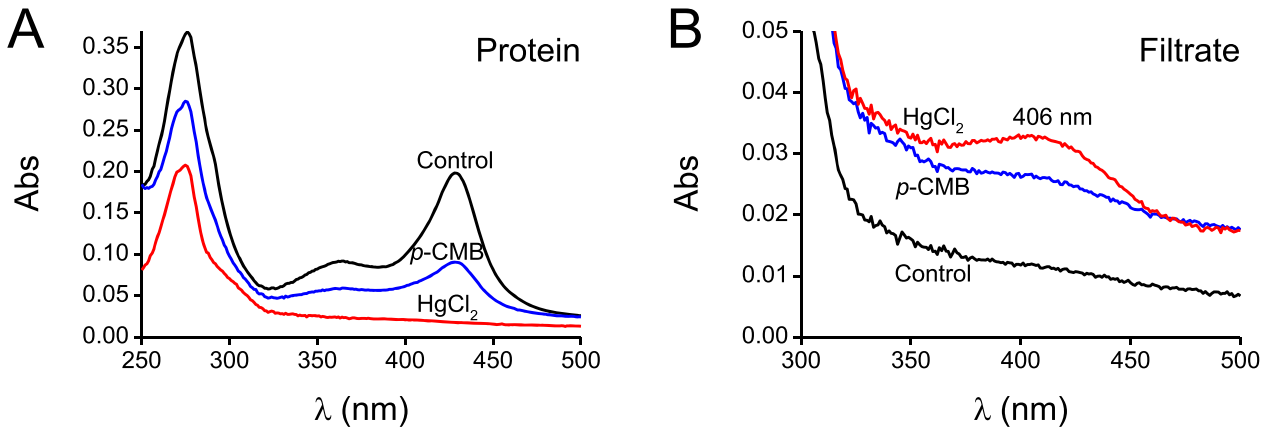

Figure 5. Treatment of CBS with mercury compounds releasing heme. Fe(III)-CBS (11 μM) was mixed with *p*-CMB (blue) or $HgCl_2$ (red) (100 μM) in Tris−HCl buffer (0.1 M, pH 7.4) at 4 °C for 48 h. (A) Absorption spectra of the protein fractions after filtration. The spectra of CBS incubated with *p*-CMB and the control without the mercury compound exhibited maxima at 280 and 428 nm. The spectrum of CBS incubated with $HgCl_2$ only showed an absorption peak at 280 nm. (B) Absorption spectra of the filtrates reveal loss of heme from $HgCl_2$-treated CBS.

compounds, we incubated 11 μM Fe(III)-CBS with 100 μM $HgCl_2$ or *p*-CMB for 48 h at 4 °C. After incubation, the samples were filtered (10 kDa cutoff). In Figure 5A, the absorption spectra of the protein fractions are compared. The sample treated with *p*-CMB still showed a peak at 428 nm after 48 h, albeit decreased in comparison to the control, suggesting that the reaction was not yet driven to completion or that washout of *p*-CMB led to recovery of the heme-thiolate coordination. In the sample treated with $HgCl_2$, the maximum at 280 nm indicated the presence of protein, but a peak attributable to heme (428 or 390 nm) was not seen. This result suggests that heme was lost from the protein. In contrast, the spectrum of the filtrate had a wide peak with an absorption maximum at ∼406 nm, compatible with the spectra reported for free hemin.[91−93] This originated from CBS samples exposed to $HgCl_2$ (Figure 5B), confirming heme release.

Effect of the Mercury Compounds on CBS Activity. Specific activities of Fe(III)-CBS exposed to *p*-CMB or $HgCl_2$ for 0.5 or 72 h at 4 °C were compared (Figure 6). As expected, the specific activity of the control sample was unaltered with time. After 0.5 h, CBS exposed to *p*-CMB was completely active, whereas after 72 h, the activity diminished to 63%. After only 0.5 h, CBS incubated with $HgCl_2$ had an activity of 38%, and after 72 h, the enzyme was almost completely inactive, in agreement with a previous report.[38]

The decrease in enzymatic activity by exposure to the mercury compounds is consistent with previous observations that perturbations in the heme coordination (*e.g.*, by site-directed mutagenesis) affect the activity. The effect has been proposed to be transduced by an α-helix that connects Cys52 with the phosphate of PLP.[30−33] In addition, the activity decreases could also be related to reactions of the mercury compounds with other protein residues.

In this work, the mercury compounds were used for mechanistic studies aimed at better understanding of the properties of the heme-thiolate in CBS. The physiological relevance of the interactions between mercury compounds and CBS is probably low. Considering that the mercury compounds lead to relatively slow decreases in enzymatic activity, their reactions with CBS are unlikely to trigger the main toxic effects. The toxicity of mercury has been related to its high affinity but relatively nonspecific binding to protein thiols, which leads to the inactivation of other key enzymes and

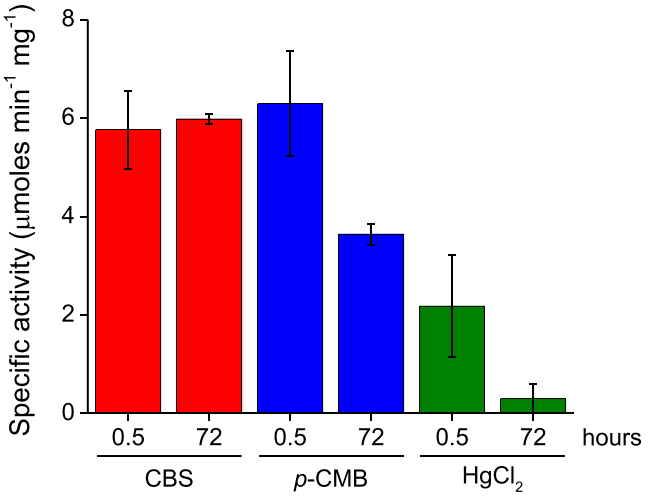

Figure 6. Specific activity of Fe(III)-CBS incubated with mercury compounds. The specific activity of Fe(III)-CBS (5.7 μM) exposed to an excess of *p*-CMB (100 μM, blue) or $HgCl_2$ (100 μM, green) for 0.5 or 72 h at 4 °C was compared with untreated controls (red). The results are reported as mean ± S.E. of duplicates of a representative experiment performed two independent times.

ion channels.[94−96] In fact, CBS was actually proposed to diminish the toxicity of methylmercury in cells through the formation of H_2S and the scavenging of methylmercury, which would thus become unavailable to react with cellular proteins.[97]

CONCLUSIONS

The reaction of Fe(III)-CBS with *p*-CMB and $HgCl_2$ is multiphasic, resulting in five-coordinate CBS lacking the thiolate coordination. In the first phase, a six-coordinate intermediate is formed, in which the original histidine and cysteine heme ligands are retained, while the cysteine is also coordinated to the mercury compound. The k_{obs1} of this phase increases hyperbolically with concentration of the mercury compound. Using either the conformational selection or induced fit model, the limiting rate constant value k_{obs1} = 0.3−0.4 s^{-1} is tentatively assigned as the weakening of the Fe−S_{Cys52} bond. The second phase is a second-order reaction with a rate constant of 0.74 ± 0.06 M^{-1} s^{-1} for *p*-CMB and 99 ± 2

https://dx.doi.org/10.1021/acsomega.0c05475
ACS Omega 2021, 6, 2192−2205

M^{-1} s^{-1} for $HgCl_2$. This phase is assigned to disruption of the heme-thiolate ligand in the reaction with *p*-CMB, where a five-coordinate heme is formed, whereas with $HgCl_2$, a new six-coordinate species is formed in which the cysteine ligand now interacts with two mercury ions in addition to heme iron. In the third phase of the reaction with $HgCl_2$, the heme-thiolate bond is disrupted in a process that is independent of the concentration of $HgCl_2$ with an apparent rate constant of $(5.9 \pm 0.6) \times 10^{-4}$ s^{-1}, forming a five-coordinate heme. Prolonged exposure of Fe(III)-CBS to $HgCl_2$ leads to heme loss from the protein and loss of enzymatic activity. In contrast, partial heme and CBS activity loss are observed upon *p*-CMB treatment.

The reaction of Fe(II)-CBS with *p*-CMB is faster than that of Fe(III)-CBS with rate constants of 40 ± 4 s^{-1} and $(6.7 \pm 0.1) \times 10^2$ M^{-1} s^{-1} for the first and second phases, respectively. The faster kinetics are consistent with the weaker $Fe-S_{Cys52}$ bond in Fe(II)-CBS. A six-coordinate intermediate is formed initially, which evolves to a five-coordinate product.

Computational simulations provided support for the feasibility of formation of complexes between CBS and the different mercury compounds, in which the cysteine remained proximal to the iron and interacted with one or two mercury compounds.

The complexity of the interactions between the mercury compounds and CBS and the formation of six-coordinate heme intermediates impeded direct determination of the rate constant for cysteine dissociation from heme. Overall, our results contribute to the understanding of the intricate effects of thiophilic mercury compounds on heme in CBS and, in general terms, to the understanding of their possible interactions with heme-thiolate proteins.

■ ASSOCIATED CONTENT

Accession Codes

The accession code for CBS is P35520.

■ AUTHOR INFORMATION

Corresponding Author

Beatriz Alvarez − *Laboratorio de Enzimología, Instituto de Química Biológica, Facultad de Ciencias, Universidad de la República, Montevideo 11400, Uruguay; Centro de Investigaciones Biomédicas (CEINBIO), Universidad de la República, Montevideo 11800, Uruguay;* orcid.org/0000-0001-6911-3132; Email: beatriz.alvarez@fcien.edu.uy

Authors

Dayana Benchoam − *Laboratorio de Enzimología, Instituto de Química Biológica, Facultad de Ciencias, Universidad de la República, Montevideo 11400, Uruguay; Centro de Investigaciones Biomédicas (CEINBIO), Universidad de la República, Montevideo 11800, Uruguay*

Ernesto Cuevasanta − *Laboratorio de Enzimología, Instituto de Química Biológica, Facultad de Ciencias, Universidad de la República, Montevideo 11400, Uruguay; Centro de Investigaciones Biomédicas (CEINBIO), Universidad de la República, Montevideo 11800, Uruguay; Unidad de Bioquímica Analítica, Centro de Investigaciones Nucleares, Facultad de Ciencias, Universidad de la República, Montevideo 11400, Uruguay*

Laia Julió Plana − *Departamento de Química Inorgánica, Analítica y Química Física, Facultad de Ciencias Exactas y Naturales, Universidad de Buenos Aires/Instituto de Química Física de los Materiales, Medio Ambiente y Energía (INQUIMAE-CONICET), C1428EGA Buenos Aires, Argentina*

Luciana Capece − *Departamento de Química Inorgánica, Analítica y Química Física, Facultad de Ciencias Exactas y Naturales, Universidad de Buenos Aires/Instituto de Química Física de los Materiales, Medio Ambiente y Energía (INQUIMAE-CONICET), C1428EGA Buenos Aires, Argentina;* orcid.org/0000-0003-3794-5713

Ruma Banerjee − *Department of Biological Chemistry, University of Michigan Medical School, Ann Arbor, Michigan 48109, United States;* orcid.org/0000-0001-8332-3275

Complete contact information is available at: https://pubs.acs.org/10.1021/acsomega.0c05475

Notes

The authors declare no competing financial interest.

■ ACKNOWLEDGMENTS

We thank Drs. David P. Ballou (University of Michigan) and Gerardo Ferrer-Sueta (Universidad de la República, Uruguay) for helpful discussions and Dr. Tatyana Spolitak (University of Michigan) for technical assistance. This work was supported in part by grants from Comisión Sectorial de Investigación Científica (Universidad de la República, Uruguay). D.B. and E.C. were partially supported by Comisión Académica de Posgrado (Universidad de la República, Uruguay) and by PEDECIBA (Uruguay). This work was supported in part by a grant from the National Institutes of Health (HL58984 to R.B.).

■ ABBREVIATIONS

CBS, cystathionine *β*-synthase; *p*-CMB, *p*-chloromercuribenzoic acid; *p*-HMB, *p*-hydroxymercuribenzoic acid; *p*-MB, *p*-mercuribenzoic acid, without chloride or hydroxyl ligands; Fe(III)-CBS, ferric CBS; Fe(II)-CBS, ferrous CBS; PLP, pyridoxal 5′-phosphate

■ REFERENCES

(1) Abe, K.; Kimura, H. The possible role of hydrogen sulfide as an endogenous neuromodulator. *J. Neurosci.* **1996**, *16*, 1066−1071.

(2) Filipovic, M. R.; Zivanovic, J.; Alvarez, B.; Banerjee, R. Chemical biology of H2S signaling through persulfidation. *Chem. Rev.* **2018**, *118*, 1253−1337.

(3) Singh, S.; Padovani, D.; Leslie, R. A.; Chiku, T.; Banerjee, R. Relative contributions of cystathionine beta-synthase and gamma-cystathionase to H2S biogenesis via alternative trans-sulfuration reactions. *J. Biol. Chem.* **2009**, *284*, 22457−22466.

(4) Ida, T.; Sawa, T.; Ihara, H.; Tsuchiya, Y.; Watanabe, Y.; Kumagai, Y.; Suematsu, M.; Motohashi, H.; Fujii, S.; Matsunaga, T.; Yamamoto, M.; Ono, K.; Devarie-Baez, N. O.; Xian, M.; Fukuto, J. M.; Akaike, T. Reactive cysteine persulfides and S-polythiolation regulate oxidative stress and redox signaling. *Proc. Natl. Acad. Sci. U. S. A.* **2014**, *111*, 7606−7611.

(5) Yadav, P. K.; Martinov, M.; Vitvitsky, V.; Seravalli, J.; Wedmann, R.; Filipovic, M. R.; Banerjee, R. Biosynthesis and reactivity of cysteine persulfides in signaling. *J. Am. Chem. Soc.* **2016**, *138*, 289−299.

(6) McCully, K. S. Vascular Pathology of homocysteinemia: Implications for the pathogenesis of arteriosclerosis. *Am. J. Pathol.* **1969**, *56*, 111−128.

(7) Mills, J. L.; Lee, Y. J.; Conley, M. R.; Kirke, P. N.; McPartlin, J. M.; Weir, D. G.; Scott, J. M. Homocysteine metabolism in pregnancies complicated by neural-tube defects. *Lancet* **1995**, *345*, 149−151.

(8) Clarke, R.; Smith, A. D.; Jobst, K. A.; Refsum, H.; Sutton, L.; Ueland, P. M. Folate, vitamin B12, and serum total homocysteine levels in confirmed Alzheimer disease. *Arch. Neurol.* **1998**, *55*, 1449−1455.
(9) Refsum, H.; Ueland, P. M.; Nygård, O.; Vollset, S. E. Homocysteine and cardiovascular disease. *Annu. Rev. Med.* **1998**, *49*, 31−62.
(10) Kraus, J. P.; Janošík, M.; Kožich, V.; Mandell, R.; Shih, V.; Sperandeo, M. P.; Sebastio, G.; de Franchis, R.; Andria, G.; Kluijtmans, L. A.; Blom, H.; Boers, G. H. J.; Gordon, R. B.; Kamoun, P.; Tsai, M. Y.; Kruger, W. D.; Koch, H. G.; Ohura, T.; Gaustadnes, M. Cystathionine beta-synthase mutations in homocystinuria. *Hum. Mutat.* **1999**, *13*, 362−375.
(11) Frank, N.; Kery, V.; Maclean, K. N.; Kraus, J. P. Solvent-Accessible cysteines in human cystathionine beta-synthase: crucial role of cysteine 431 in S-adenosyl-L-methionine binding. *Biochemistry* **2006**, *45*, 11021−11029.
(12) Sen, S.; Banerjee, R. A pathogenic linked mutation in the catalytic core of human cystathionine beta-synthase disrupts allosteric regulation and allows kinetic characterization of a full-length dimer. *Biochemistry* **2007**, *46*, 4110−4116.
(13) Ereño-Orbea, J.; Majtan, T.; Oyenarte, I.; Kraus, J. P.; Martínez-Cruz, L. A. Structural basis of regulation and oligomerization of human cystathionine *β*-synthase, the central enzyme of transsulfuration. *Proc. Natl. Acad. Sci. U. S. A.* **2013**, *110*, E3790−E3799.
(14) Majtan, T.; Pey, A. L.; Fernández, R.; Fernández, J. A.; Martínez-Cruz, L. A.; Kraus, J. P. Domain organization, catalysis and regulation of eukaryotic cystathionine beta-synthases. *PLoS One* **2014**, *9*, No. e105290.
(15) Kraus, J. P.; Le, K.; Swaroop, M.; Ohura, T.; Tahara, T.; Rosenberg, L. E.; Roper, M. D.; Kožich, V. Human cystathionine beta-synthase cDNA: Sequence, alternative splicing and expression in cultured cells. *Hum. Mol. Genet.* **1993**, *2*, 1633−1638.
(16) Kraus, J.; Packman, S.; Fowler, B.; Rosenberg, L. E. Purification and properties of cystathionine beta-synthase from human liver. evidence for identical subunits. *J. Biol. Chem.* **1978**, *253*, 6523−6528.
(17) Kery, V.; Bukovska, G.; Kraus, J. P. Transsulfuration depends on heme in addition to pyridoxal 5′-phosphate. cystathionine beta-synthase is a heme protein. *J. Biol. Chem.* **1994**, *269*, 25283−25288.
(18) Taoka, S.; Widjaja, L.; Banerjee, R. Assignment of enzymatic functions to specific regions of the plp-dependent heme protein cystathionine beta-synthase. *Biochemistry* **1999**, *38*, 13155−13161.
(19) Kumar, A.; Wißbrock, A.; Goradia, N.; Bellstedt, P.; Ramachandran, R.; Imhof, D.; Ohlenschläger, O. Heme interaction of the intrinsically disordered n-terminal peptide segment of human cystathionine-*β*-synthase. *Sci. Rep.* **2018**, *8*, 2474.
(20) Finkelstein, J. D.; Kyle, W. E.; Martin, J. L.; Pick, A.-M. Activation of cystathionine synthase by adenosylmethionine and adenosylethionine. *Biochem. Biophys. Res. Commun.* **1975**, *66*, 81−87.
(21) Ojha, S.; Hwang, J.; Kabil, Ö.; Penner-Hahn, J. E.; Banerjee, R. Characterization of the heme in human cystathionine *β*-synthase by X-ray absorption and electron paramagnetic resonance spectroscopies. *Biochemistry* **2000**, *39*, 10542−10547.
(22) Omura, T.; Sadano, H.; Hasegawa, T.; Yoshida, Y.; Kominami, S. Hemoprotein H-450 identified as a form of cytochrome p-450 having an endogenous ligand at the 6th coordination position of the heme. *J. Food Biochem.* **1984**, *96*, 1491−1500.
(23) Meier, M.; Janosik, M.; Kery, V.; Kraus, J. P.; Burkhard, P. Structure of human cystathionine beta-synthase: a unique pyridoxal 5′-phosphate-dependent heme protein. *EMBO J.* **2001**, *20*, 3910−3916.
(24) Taoka, S.; Lepore, B. W.; Kabil, Ö.; Ojha, S.; Ringe, D.; Banerjee, R. Human cystathionine beta-synthase is a heme sensor protein. Evidence that the redox sensor is heme and not the vicinal cysteines in the CXXC motif seen in the crystal structure of the truncated enzyme. *Biochemistry* **2002**, *41*, 10454−10461.
(25) Cuevasanta, E.; Carballal, S.; Graña, M.; Alvarez, B. The redox properties of the unique heme in cystathionine *β*-synthase. *BioInorg. React. Mech.* **2014**, *9*, 27−34.
(26) Kabil, Ö.; Toaka, S.; LoBrutto, R.; Shoemaker, R.; Banerjee, R. Pyridoxal phosphate binding sites are similar in human heme-dependent and yeast heme-independent cystathionine *β*-synthases Evidence from ^{31}P NMR and pulsed EPR spectroscopy that heme and PLP cofactors are not proximal in the human enzyme. *J. Biol. Chem.* **2001**, *276*, 19350−19355.
(27) Jhee, K. H.; McPhie, P.; Miles, E. W. Yeast cystathionine *β*-synthase is a pyridoxal phosphate enzyme but, unlike the human enzyme, is not a heme protein. *J. Biol. Chem.* **2000**, *275*, 11541−11544.
(28) Nozaki, T.; Shigeta, Y.; Saito-Nakano, Y.; Imada, M.; Kruger, W. D. Characterization of transsulfuration and cysteine biosynthetic pathways in the protozoan hemoflagellate, *Trypanosoma cruzi* Isolation and molecular characterization of cystathionine beta-synthase and serine acetyltransferase from trypanosoma. *J. Biol. Chem.* **2001**, *276*, 6516−6523.
(29) Majtan, T.; Singh, L. R.; Wang, L.; Kruger, W. D.; Kraus, J. P. Active cystathionine beta-synthase can be expressed in heme-free systems in the presence of metal-substituted porphyrins or a chemical chaperone. *J. Biol. Chem.* **2008**, *283*, 34588−34595.
(30) Singh, S.; Madzelan, P.; Stasser, J.; Weeks, C. L.; Becker, D.; Spiro, T. G.; Penner-Hahn, J.; Banerjee, R. Modulation of the heme electronic structure and cystathionine beta-synthase activity by second coordination sphere ligands: The role of heme ligand switching in redox regulation. *J. Inorg. Biochem.* **2009**, *103*, 689−697.
(31) Weeks, C. L.; Singh, S.; Madzelan, P.; Banerjee, R.; Spiro, T. G. Heme regulation of human cystathionine beta-synthase activity: Insights from fluorescence and Raman spectroscopy. *J. Am. Chem. Soc.* **2009**, *131*, 12809−12816.
(32) Smith, A. T.; Su, Y.; Stevens, D. J.; Majtan, T.; Kraus, J. P.; Burstyn, J. N. Effect of the disease-causing R266K mutation on the heme and PLP environments of human cystathionine *β*-synthase. *Biochemistry* **2012**, *51*, 6360−6370.
(33) Yadav, P. K.; Xie, P.; Banerjee, R. Allosteric communication between the pyridoxal 5′-phosphate (PLP) and heme sites in the H2S generator human cystathionine *β*-synthase. *J. Biol. Chem.* **2012**, *287*, 37611−37620.
(34) Kery, V.; Poneleit, L.; Kraus, J. P. Trypsin cleavage of human cystathionine beta-synthase into an evolutionarily conserved active core: Structural and functional consequences. *Arch. Biochem. Biophys.* **1998**, *355*, 222−232.
(35) Janosik, M.; Meier, M.; Kery, V.; Oliveriusova, J.; Burkhard, P.; Kraus, J. P. Crystallization and preliminary X-ray diffraction analysis of the active core of human recombinant cystathionine *β*-synthase: An enzyme involved in vascular disease. *Acta Crystallogr., Sect. D: Biol. Crystallogr.* **2001**, *57*, 289−291.
(36) Kim, I.-C.; Deal, W. C., Jr. Isolation and properties of a new, soluble, hemoprotein (H-450) from pig liver. *Biochemistry* **1976**, *15*, 4925−4930.
(37) Taoka, S.; Ohja, S.; Shan, X.; Kruger, W. D.; Banerjee, R. Evidence for heme-mediated redox regulation of human cystathionine *β*-synthase activity. *J. Biol. Chem.* **1998**, *273*, 25179−25184.
(38) Taoka, S.; Green, E. L.; Loehr, T. M.; Banerjee, R. Mercuric chloride-induced spin or ligation state changes in ferric or ferrous human cystathionine beta-synthase inhibit enzyme activity. *J. Inorg. Biochem.* **2001**, *87*, 253−259.
(39) Celano, L.; Gil, M.; Carballal, S.; Durán, R.; Denicola, A.; Banerjee, R.; Alvarez, B. Inactivation of cystathionine beta-synthase with peroxynitrite. *Arch. Biochem. Biophys.* **2009**, *491*, 96−105.
(40) Vadon-Le Goff, S.; Delaforge, M.; Boucher, J. L.; Janosik, M.; Kraus, J. P.; Mansuy, D. Coordination chemistry of the heme in cystathionine beta-synthase: formation of iron(ii)-isonitrile complexes. *Biochem. Biophys. Res. Commun.* **2001**, *283*, 487−492.
(41) Vicente, J. B.; Colaço, H. G.; Mendes, M. I. S.; Sarti, P.; Leandro, P.; Giuffrè, A. NO* binds human cystathionine *β*-synthase quickly and tightly. *J. Biol. Chem.* **2014**, *289*, 8579−8587.

https://dx.doi.org/10.1021/acsomega.0c05475
ACS Omega 2021, 6, 2192−2205

(42) Carballal, S.; Cuevasanta, E.; Marmisolle, I.; Kabil, O.; Gherasim, C.; Ballou, D. P.; Banerjee, R.; Alvarez, B. Kinetics of reversible reductive carbonylation of heme in human cystathionine β-synthase. *Biochemistry* **2013**, *52*, 4553−4562.
(43) Kabil, O.; Weeks, C. L.; Carballal, S.; Gherasim, C.; Alvarez, B.; Spiro, T. G.; Banerjee, R. Reversible heme-dependent regulation of human cystathionine β-synthase by a flavoprotein oxidoreductase. *Biochemistry* **2011**, *50*, 8261−8263.
(44) Carballal, S.; Madzelan, P.; Zinola, C. F.; Graña, M.; Radi, R.; Banerjee, R.; Alvarez, B. Dioxygen reactivity and heme redox potential of truncated human cystathionine beta-synthase. *Biochemistry* **2008**, *47*, 3194−3201.
(45) Puranik, M.; Weeks, C. L.; Lahaye, D.; Kabil, O.; Taoka, S.; Nielsen, S. B.; Groves, J. T.; Banerjee, R.; Spiro, T. G. Dynamics of carbon monoxide binding to cystathionine beta-synthase. *J. Biol. Chem.* **2006**, *281*, 13433−13438.
(46) Taoka, S.; West, M.; Banerjee, R. Characterization of the heme and pyridoxal phosphate cofactors of human cystathionine beta-synthase reveals nonequivalent active sites. *Biochemistry* **1999**, *38*, 2738−2744.
(47) Taoka, S.; Banerjee, R. Characterization of NO binding to human cystathionine beta-synthase: Possible implications of the effects of CO and NO binding to the human enzyme. *J. Inorg. Biochem.* **2001**, *87*, 245−251.
(48) Carballal, S.; Cuevasanta, E.; Yadav, P. K.; Gherasim, C.; Ballou, D. P.; Alvarez, B.; Banerjee, R. Kinetics of nitrite reduction and peroxynitrite formation by ferrous heme in human cystathionine β-synthase. *J. Biol. Chem.* 2016, DOI: 10.1074/jbc.M116.718734.
(49) Gherasim, C.; Yadav, P. K.; Kabil, O.; Niu, W.-N.; Banerjee, R. Nitrite reductase activity and inhibition of H_2S biogenesis by human cystathionine β-synthase. *PLoS One* **2014**, *9*, No. e85544.
(50) Hasegawa, T.; Sadano, H.; Omura, T. Spectral similarities between "H-450" and cytochrome P-450. *J. Biochem.* **1984**, *96*, 265−268.
(51) Pazicni, S.; Cherney, M. M.; Lukat-Rodgers, G. S.; Oliveriusová, J.; Rodgers, K. R.; Kraus, J. P.; Burstyn, J. N. The heme of cystathionine beta-synthase likely undergoes a thermally induced redox-mediated ligand switch. *Biochemistry* **2005**, *44*, 16785−16795.
(52) Cherney, M. M.; Pazicni, S.; Frank, N.; Marvin, K. A.; Kraus, J. P.; Burstyn, J. N. Ferrous human cystathionine beta-synthase loses activity during enzyme assay due to a ligand switch process. *Biochemistry* **2007**, *46*, 13199−13210.
(53) Vicente, J. B.; Colaço, H. G.; Sarti, P.; Leandro, P.; Giuffrè, A. S-adenosyl-L-methionine modulates CO and NO• binding to the human H2S-generating enzyme cystathionine β-synthase. *J. Biol. Chem.* **2016**, *291*, 572−581.
(54) Prathapasinghe, G. A.; Siow, Y. L.; Xu, Z.; O, K. Inhibition of cystathionine-β-synthase activity during renal ischemia-reperfusion: Role of pH and nitric oxide. *Am. J. Physiol.: Renal. Physiol.* **2008**, *295*, F912−F922.
(55) Shintani, T.; Iwabuchi, T.; Soga, T.; Kato, Y.; Yamamoto, T.; Takano, N.; Hishiki, T.; Ueno, Y.; Ikeda, S.; Sakuragawa, T.; Ishikawa, K.; Goda, N.; Kitagawa, Y.; Kajimura, M.; Matsumoto, K.; Suematsu, M. Cystathionine beta-synthase as a carbon monoxide-sensitive regulator of bile excretion. *Hepatology* **2009**, *49*, 141−150.
(56) Morikawa, T.; Kajimura, M.; Nakamura, T.; Hishiki, T.; Nakanishi, T.; Yukutake, Y.; Nagahata, Y.; Ishikawa, M.; Hattori, K.; Takenouchi, T.; Takahashi, T.; Ishii, I.; Matsubara, K.; Kabe, Y.; Uchiyama, S.; Nagata, E.; Gadalla, M. M.; Snyder, S. H.; Suematsu, M. Hypoxic regulation of the cerebral microcirculation is mediated by a carbon monoxide-sensitive hydrogen sulfide pathway. *Proc. Natl. Acad. Sci. U. S. A.* **2012**, *109*, 1293−1298.
(57) Yamamoto, T.; Takano, N.; Ishiwata, K.; Ohmura, M.; Nagahata, Y.; Matsuura, T.; Kamata, A.; Sakamoto, K.; Nakanishi, T.; Kubo, A.; Hishiki, T.; Suematsu, M. Reduced methylation of PFKFB3 in cancer cells shunts glucose towards the pentose phosphate pathway. *Nat. Commun.* **2014**, *5*, 3480.
(58) Kabil, O.; Yadav, V.; Banerjee, R. Heme-dependent metabolite switching regulates H2S synthesis in response to endoplasmic reticulum (ER) stress. *J. Biol. Chem.* **2016**, *291*, 16418−16423.
(59) Vicente, J. B.; Colaço, H. G.; Malagrinò, F.; Santo, P. E.; Gutierres, A.; Bandeiras, T. M.; Leandro, P.; Brito, J. A.; Giuffrè, A. A clinically relevant variant of the human hydrogen sulfide-synthesizing enzyme cystathionine β-synthase: Increased CO reactivity as a novel molecular mechanism of pathogenicity? *Oxid. Med. Cell. Longevity* 2017, *2017*, 8940321, DOI: 10.1155/2017/8940321.
(60) Niu, W.; Wang, J.; Qian, J.; Wang, M.; Wu, P.; Chen, F.; Yan, S. Allosteric control of human cystathionine β-synthase activity by a redox active disulfide bond. *J. Biol. Chem.* **2018**, *293*, 2523−2533.
(61) Kashiwamata, S.; Greenberg, D. M. Studies on cystathionine synthase of rat liver. Properties of the highly purified enzyme. *Biochim. Biophys. Acta* **1970**, *212*, 488−500.
(62) Burgot, J. L. *Ionic Equilibria in Analytical Chemistry*; Springer-Verlag: New York, 2012.
(63) Rabenstein, D. L. The aqueous solution chemistry of methylmercury and its complexes. *Acc. Chem. Res.* **1978**, *11*, 100−107.
(64) Rabenstein, D. L.; Isab, A. A. A proton nuclear magnetic resonance study of the interaction of mercury with intact human erythrocytes. *Biochim. Biophys. Acta, Mol. Cell Res.* **1982**, *721*, 374−384.
(65) Patil, P. V.; Ballou, D. P. The use of protocatechuate dioxygenase for maintaining anaerobic conditions in biochemical experiments. *Anal. Biochem.* **2000**, *286*, 187−192.
(66) Frisch, M. J.; Trucks, G. W.; Schlegel, H. B.; Scuseria, G. E.; Robb, M. A.; Cheeseman, J. R.; Montgomery, J. A., Jr.; Vreven, T.; Kudin, K. N.; Burant, J. C. *Gaussian 03*, Gaussian, Inc.: Wallingford, CT, 2004.
(67) Perdew, J. P.; Burke, K.; Ernzerhof, M. Generalized gradient approximation made simple. *Phys. Rev. Lett.* **1996**, *77*, 3865.
(68) Crespo, A.; Scherlis, D. A.; Martí, M. A.; Ordejón, P.; Roitberg, A. E.; Estrin, D. A. A DFT-based QM-MM approach designed for the treatment of large molecular systems: Application to chorismate mutase. *J. Phys. Chem. B* **2003**, *107*, 13728−13736.
(69) Crespo, A.; Martí, M. A.; Estrin, D. A.; Roitberg, A. E. Multiple-steering QM−MM calculation of the free energy profile in chorismate mutase. *J. Am. Chem. Soc.* **2005**, *127*, 6940−6941.
(70) Lindorff-Larsen, K.; Piana, S.; Palmo, K.; Maragakis, P.; Klepeis, J. L.; Dror, R. O.; Shaw, D. E. Improved side-chain torsion potentials for the Amber Ff99SB protein force field. *Proteins: Struct., Funct., Bioinf.* **2010**, *78*, 1950−1958.
(71) Eichinger, M.; Tavan, P.; Hutter, J.; Parrinello, M. A hybrid method for solutes in complex solvents: Density functional theory combined with empirical force fields. *J. Chem. Phys.* **1999**, *110*, 10452−10467.
(72) Ereño-Orbea, J.; Majtan, T.; Oyenarte, I.; Kraus, J. P.; Martínez-Cruz, L. A. Structural insight into the molecular mechanism of allosteric activation of human cystathionine β-synthase by S-adenosylmethionine. *Proc. Natl. Acad. Sci. U. S. A.* **2014**, *111*, E3845−E3852.
(73) Marti, M. A.; Crespo, A.; Capece, L.; Boechi, L.; Bikiel, D. E.; Scherlis, D. A.; Estrin, D. A. Dioxygen affinity in heme proteins investigated by computer simulation. *J. Inorg. Biochem.* **2006**, *100*, 761−770.
(74) Capece, L.; Marti, M. A.; Crespo, A.; Doctorovich, F.; Estrin, D. A. Heme protein oxygen affinity regulation exerted by proximal effects. *J. Am. Chem. Soc.* **2006**, *128*, 12455−12461.
(75) Capece, L.; Boechi, L.; Perissinotti, L. L.; Arroyo-Mañez, P.; Bikiel, D. E.; Smulevich, G.; Marti, M. A.; Estrin, D. A. Small ligand−globin interactions: Reviewing lessons derived from computer simulation. *Biochim. Biophys. Acta, Proteins Proteomics* **2013**, *1834*, 1722−1738.
(76) Viappiani, C.; Abbruzzetti, S.; Ronda, L.; Bettati, S.; Henry, E. R.; Mozzarelli, A.; Eaton, W. A. Experimental basis for a new allosteric model for multisubunit proteins. *Proc. Natl. Acad. Sci.* **2014**, *111*, 12758−12763.

https://dx.doi.org/10.1021/acsomega.0c05475
ACS Omega 2021, 6, 2192−2205

(77) Brewitz, H. H.; Kühl, T.; Goradia, N.; Galler, K.; Popp, J.; Neugebauer, U.; Ohlenschläger, O.; Imhof, D. Role of the chemical environment beyond the coordination site: structural insight into Fe(III) protoporphyrin binding to cysteine-based heme-regulatory protein motifs. *Chembiochem* **2015**, *16*, 2216−2224.
(78) Brewitz, H. H.; Goradia, N.; Schubert, E.; Galler, K.; Kühl, T.; Syllwasschy, B.; Popp, J.; Neugebauer, U.; Hagelueken, G.; Schiemann, O.; Ohlenschläger, O.; Imhof, D. Heme interacts with histidine- and tyrosine-based protein motifs and inhibits enzymatic activity of chloramphenicol acetyltransferase from *Escherichia coli*. *Biochim. Biophys. Acta* **2016**, *1860*, 1343−1353.
(79) Sono, M.; Stuehr, D. J.; Ikeda-Saito, M.; Dawson, J. H. Identification of nitric oxide synthase as a thiolate-ligated heme protein using magnetic circular dichroism spectroscopy Comparison with cytochrome P-450-CAM and chloroperoxidase. *J. Biol. Chem.* **1995**, *270*, 19943−19948.
(80) Gupta, N.; Ragsdale, S. W. Thiol-disulfide redox dependence of heme binding and heme ligand switching in nuclear hormone receptor Rev-Erbβ. *J. Biol. Chem.* **2011**, *286*, 4392−4403.
(81) de Rosny, E.; de Groot, A.; Jullian-Binard, C.; Gaillard, J.; Borel, F.; Pebay-Peyroula, E.; Fontecilla-Camps, J. C.; Jouve, H. M. *Drosophila* nuclear receptor E75 is a thiolate hemoprotein. *Biochemistry* **2006**, *45*, 9727−9734.
(82) Ojha, S.; Wu, J.; LoBrutto, R.; Banerjee, R. Effects of heme ligand mutations including a pathogenic variant, H65R, on the properties of human cystathionine β-synthase. *Biochemistry* **2002**, *41*, 4649−4654.
(83) Marvin, K. A.; Kerby, R. L.; Youn, H.; Roberts, G. P.; Burstyn, J. N. The transcription regulator RcoM-2 from *Burkholderia xenovorans* is a cysteine-ligated hemoprotein that undergoes a redox-mediated ligand switch. *Biochemistry* **2008**, *47*, 9016−9028.
(84) Dewilde, S.; Kiger, L.; Burmester, T.; Hankeln, T.; Baudin-Creuza, V.; Aerts, T.; Marden, M. C.; Caubergs, R.; Moens, L. Biochemical characterization and ligand binding properties of neuroglobin, a novel member of the globin family. *J. Biol. Chem.* **2001**, *276*, 38949−38955.
(85) Hammes, G. G.; Chang, Y.-C.; Oas, T. G. Conformational selection or induced fit: A flux description of reaction mechanism. *Proc. Natl. Acad. Sci. U. S. A.* **2009**, *106*, 13737−13741.
(86) Vogt, A. D.; Di Cera, E. Conformational selection or induced fit? A critical appraisal of the kinetic mechanism. *Biochemistry* **2012**, *51*, 5894−5902.
(87) Rabenstein, D. L.; Fairhurst, M. T. Nuclear magnetic resonance studies of the solution chemistry of metal complexes. XI. The binding of methylmercury by sulfhydryl-containing amino acids and by glutathione. *J. Am. Chem. Soc.* **1975**, *97*, 2086−2092.
(88) Simpson, P. G.; Hopkins, T. E.; Haque, R. Binding of methylmercury chloride to the model peptide, N-acetyl-L-cysteine. proton magnetic resonance study. *J. Phys. Chem.* **1973**, *77*, 2282−2285.
(89) Taylor, N. J.; Carty, A. J. Nature of Hg+−L-cysteine complexes implicated in mercury biochemistry. *J. Am. Chem. Soc.* **1977**, *99*, 6143−6145.
(90) Dent, M. R.; Milbauer, M. W.; Hunt, A. P.; Aristov, M. M.; Guzei, I. A.; Lehnert, N.; Burstyn, J. N. Electron paramagnetic resonance spectroscopy as a probe of hydrogen bonding in heme-thiolate proteins. *Inorg. Chem.* **2019**, *58*, 16011−16027.
(91) Karnaukhova, E.; Rutardottir, S.; Rajabi, M.; Wester Rosenlöf, L.; Alayash, A. I.; Åkerström, B. Characterization of heme binding to recombinant α_1-microglobulin. *Front. Physiol.* **2014**, *5*, 465.
(92) Georgiou-Siafis, S. K.; Samiotaki, M. K.; Demopoulos, V. J.; Panayotou, G.; Tsiftsoglou, A. S. Formation of novel N-acetylcysteine-hemin adducts abrogates hemin-induced cytotoxicity and suppresses the NRF2-driven stress response in human pro-erythroid K562 cells. *Eur. J. Pharmacol.* **2020**, *880*, 173077.
(93) Hannibal, L.; Collins, D.; Brassard, J.; Chakravarti, R.; Vempati, R.; Dorlet, P.; Santolini, J.; Dawson, J. H.; Stuehr, D. J. Heme binding properties of glyceraldehyde-3-phosphate dehydrogenase. *Biochemistry* **2012**, *51*, 8514−8529.
(94) Clarkson, T. W.; Magos, L. The toxicology of mercury and its chemical compounds. *Crit. Rev. Toxicol.* **2008**, *36*, 609−662.
(95) Ynalvez, R.; Gutierrez, J.; Gonzalez-Cantu, H. Mini-review: Toxicity of mercury as a consequence of enzyme alteration. *Biometals* **2016**, *29*, 781−788.
(96) Yang, L.; Zhang, Y.; Wang, F.; Luo, Z.; Guo, S.; Strähle, U. Toxicity of mercury: Molecular evidence. *Chemosphere* **2020**, *245*, 125586.
(97) Yoshida, E.; Toyama, T.; Shinkai, Y.; Sawa, T.; Akaike, T.; Kumagai, Y. Detoxification of methylmercury by hydrogen sulfide-producing enzyme in mammalian cells. *Chem. Res. Toxicol.* **2011**, *24*, 1633−1635.

https://dx.doi.org/10.1021/acsomega.0c05475
ACS Omega 2021, 6, 2192−2205